ChemComm

COMMUNICATION

View Article Online
View Journal | View Issue

Cite this: *Chem. Commun.*, 2019, **55**, 3331

Received 2nd January 2019,
Accepted 19th February 2019

DOI: 10.1039/c9cc00038k

rsc.li/chemcomm

Mn_2CoReO_6: a robust multisublattice antiferromagnetic perovskite with small A-site cations†

Corey E. Frank,[a] Emma E. McCabe,[b] Fabio Orlandi,[c] Pascal Manuel,[c] Xiaoyan Tan,[d] Zheng Deng,[e] Mark Croft,[f] Vanessa Cascos,[b] Thomas Emge,[a] Hai L. Feng,[a] Saul Lapidus,[g] Changqing Jin,[e] MeiXia Wu,[h] Man Rong Li,[h] Steven Ehrlich,[i] Syed Khalid,[i] Nicholas Quackenbush,[j] Shuang Yu,[e] David Walker[k] and Martha Greenblatt *[a]

Mn_2CoReO_6, the fourth known magnetic transition-metal-only double perovskite oxide (space group $P2_1/n$) was synthesized at high pressure and temperature (8 GPa, 1350 °C). Large structural distortions are induced by the small A-site Mn^{2+} cations. Mn_2CoReO_6 exhibits complex magnetic properties with a robust antiferromagnetic order (T_N = 94 K) involving all cation sublattices.

The search for new materials with potential spintronics applications is increasingly important to the future of microelectronics as the limit of Moore's Law approaches.[1,2] Double perovskite (DP) oxides ($A_2BB'O_6$) (A = alkali or rare earth metal, B = 3d transition metal, B′ = 4d/5d transition metal) have been particularly important to this search since the discovery of Sr_2FeMoO_6.[3–8] The interesting magnetic and transport properties in these materials are primarily driven by interactions between the B and B′-cations, for which large spin orbit coupling and spin polarization of a late transition metal appears to be required.[9,10]

In an archetypical DP, a large A-cation is 12-fold coordinated by oxygen while the smaller B-cations form a three dimensional (3D) array of corner sharing $B/B'O_6$ octahedra. DPs in which A and B are of similar size (possible through $B/B'O_6$ tilting) are known to exhibit large structural distortions and distinct magneto-structural coupling behaviours. While there are exceptions, DPs with small A-site cations frequently require high pressure (>3 GPa) and temperature for their synthesis.[11–14]

In the so-far-rare cases in which all cations are transition metals, multiple magnetic sublattices can arise with unusual and intense interactions.[15–20] In this work, we present the fourth transition-metal-only DP (TMO-DP), Mn_2CoReO_6. Co and Re were selected as the B and B′ site cations due to the interesting magnetic interactions exhibited in A_2CoReO_6 DPs such as Pb_2CoReO_6.[21–24] Small black, plate-like crystals of Mn_2CoReO_6 were synthesized at high pressure and temperature (8 GPa, 1625 K) in a Walker-Type multi-anvil device.

Analysis of neutron powder diffraction (NPD) data revealed a trace of spinel-like impurity (Mn_3O_4 or $Mn_{3-x}Co_xO_4$)[25] which was included in refinements. Refinements indicated that the crystal structure of Mn_2CoReO_6 (space group $P2_1/n$) is analogous to preceding TMO-DPs Mn_2MnReO_6, Mn_2FeReO_6, and $Mn_2(Fe_{0.8}Mo_{0.2})MoO_6$[17,18,20] and to non-magnetic A site A_2MnReO_6 (A = Ca, Sr) phases[26,27] (see ESI† for concurring single crystal and powder X-ray and synchrotron results). Good contrast in neutron scattering lengths of the cations[28] means that NPD data are sensitive to antisite disorder. Refinements revealed almost complete ordering of Co and Re on the B/B′ sites (referred to as Co_B and $Re_{B'}$), and ~16% disorder between Mn on the A site (Mn_A) and Co on the B site. The crystal structure has significant octahedral tilts, with Co–O–Re angles between 135°–142° (relative to 180°). These tilts ($a^-a^-c^+$ in Glazer notation) are similar to those in previous TMO-DPs[17,18,20] and noticeably larger than those in A_2MnReO_6 (A = Ca, Sr).[26,27] Large tilting optimises bonding around the small Mn^{2+} ion (0.96 Å, 8-coordinate)[29] on the

[a] *Department of Chemistry and Chemical Biology, Rutgers, The State University of New Jersey, Piscataway, New Jersey, 08854, USA. E-mail: greenbla@chem.rutgers.edu*
[b] *School of Physical Sciences, University of Kent, Canterbury, Kent, CT2 7NH, UK*
[c] *ISIS Facility, STFC, Rutherford Appleton Laboratory, Chilton, Didcot, Oxfordshire, OX11 0QX, UK*
[d] *Department of Chemistry and Biochemistry, George Mason University, Virginia, 22030, USA*
[e] *Institute of Physics, School of Physics, University of Chinese Sciences, P. O. Box 603, Beijing, 100190, P. R. China*
[f] *Department of Physics and Astronomy, Rutgers, The State University of New Jersey, Piscataway, New Jersey, 08854, USA*
[g] *Advanced Photon Source, Argonne National Laboratory, Argonne, Illinois, 60439, USA*
[h] *MOE Key Laboratory of Bioinorganic and Synthetic Chemistry, School of Chemistry, Sun Yat-Sen University, Guangzhou 510275, China*
[i] *NSLS-II, Brookhaven National Laboratory, Upton, NY, USA*
[j] *Materials Measurement Science Division, Material Measurement Laboratory, National Institute of Standards and Technology, Gaithersburg, MD 20899, USA*
[k] *Lamont Doherty Earth Observatory, Columbia University, Palisades, New York, 10964, USA*

† Electronic supplementary information (ESI) available. CCDC 1888374. For ESI and crystallographic data in CIF or other electronic format see DOI: 10.1039/c9cc00038k

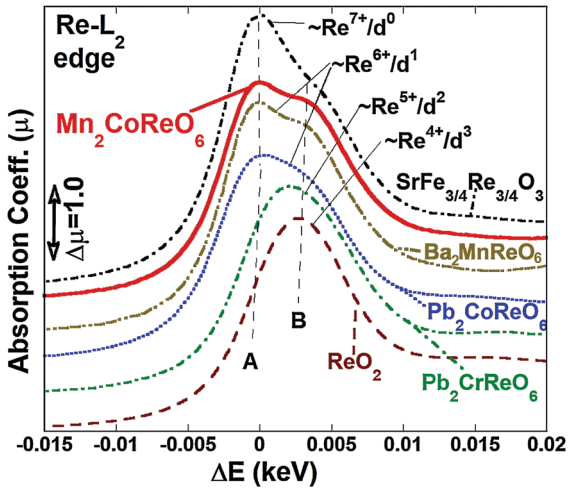

Fig. 1 The Re-L_2 edge for Mn_2CoReO_6 compared to those of other standard octahedral Re–O compounds (spanning Re^{7+}/d^0 to Re^{4+}/d^3). Spectra have been shifted in energy to approximately align the B (e_g-hole-related) features. The zero of the relative energy scale (ΔE) was chosen as the nominal position of the A (t_{2g}-hole-related) features. Spectra have been displaced vertically for clarity.

A site and emphasises the difficulty in introducing small A-site ions into the perovskite lattice. The average Re–O bond length (1.939(2) Å at 200 K) observed for Mn_2CoReO_6 is similar to that observed for Mn_2MnReO_6 (1.930(2) Å at 300 K)[17] containing Re^{6+}, and shorter than that observed in Mn_2FeReO_6 (1.961(9) Å), which contains both Re^{6+} and Re^{5+}.[18] X-ray absorption near-edge spectroscopy (XANES) was used to investigate the transition metal oxidation states and analysis of the Mn and Co K-edges (and pre-edge features) suggested that both are in 2+ oxidation states, while the Re-$L_{2,3}$ edges (Fig. 1 and ESI6.3, ESI†) were consistent with Re^{6+} ($5d^1$).

Magnetic susceptibility (χ) measurements (Fig. 2) show a local maximum at 94 K, which coincides with the asymmetric peak in heat capacity (Fig. ESI9.1, ESI†), suggesting long-range magnetic order below T_N = 94 K, while below ~50 K, field-cooled and zero-field-cooled (FC and ZFC) measurements diverge. At high

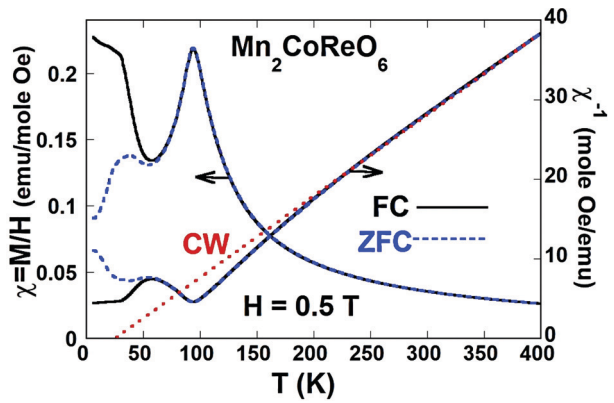

Fig. 2 The H = 0.5 T, temperature dependent magnetic susceptibility, χ, and the inverse susceptibilities, χ^{-1}, for Mn_2CoReO_6 collected under field cooled (FC) and zero field cooled (ZFC) conditions. The Curie Weiss (CW) fit to the high temperature χ^{-1} data is indicated by a dotted line.

temperatures, χ^{-1} is close to CW behaviour and suggests a paramagnetic moment of 8.84 μ_B per formula unit and a positive intercept (Weiss temperature) of 25.6 K. The paramagnetic moment is slightly lower than the theoretical moment for Mn_2CoReO_6 (9.38 μ_B) and may reflect a slight reduction in Re^{6+} moment due to spin–orbit coupling. The positive x axis intercept of χ^{-1} may indicate some underlying ferromagnetic (FM) interactions (despite long-range AFM order), although the temperature dependence of χ may also arise from crystal field effects as reported for Sr_2CoReO_6[22] or be influenced by the presence of a trace ferrimagnetic Mn_3O_4-like phase.

Magnetisation measurements were also carried out as a function of applied field (Fig. ESI7.1, ESI†) and indicate very robust AFM order below 94 K with only a very slight decrease in T_N at higher fields. This implies that magneto-crystalline anisotropy appears strong enough that the applied H-field is unable to induce any significant continuous canting of the AFM order away from its preferred crystalline ordering direction.

Isothermal magnetization measurements (Fig. ESI7.1, ESI†) are consistent with paramagnetic behaviour for $T \geq 150$ K. At lower temperatures, magnetization *vs.* field is not linear. At 5 K, magnetization varies smoothly with field (giving no evidence for a field-induced magnetic transition), but gives a small total magnetization (~1 μ_B, more than an order of magnitude less than the potential 13.5 μ_B per f.u.), consistent with the modest field response within an AFM state, small remnant magnetization (~0.1 μ_B), and a coercive field of ~ 0.5 T. There are several possible explanations for this magnetization behaviour at low temperatures, including the presence of trace amounts of a ferrimagnetic phase as noted above. It is also possible that some form of spin reorientation transition (or evolution) is active in this temperature range. A change in the Re contribution in the magnetic order is also possible. Such changes are not inconsistent with the temperature dependent NPD results and are discussed further below. It is also possible that AFM domain effects are responsible for this $T < 50$ K magnetic behavior. The NPD refinement found an ~16% antisite disorder between A-site Mn and B-site Co. Such interchanging of S = 5/2 and 3/2 at sites allows for a local uncompensated moment that, when coupled to other disorder effects, can enhance the coupling of external magnetic field. Above T_N, AFM fluctuations with modest net magnetic moments would respond to an external field and could motivate the FM components observed in χ^{-1} for $T > T_N$ (see Fig. 2) and in the $M(H)$ at 100 K (see Fig. ESI7.1, ESI†). Similarly, FC conditions would lead to a nucleation and growth of AFM domains with larger net moments aligned with the field, whereas ZFC conditions would lead to a low-magnetization/random-domain growth.

The electrical resistivity of Mn_2CoReO_6 was measured and increased smoothly on cooling (Fig. ESI8.1, ESI†). The zero-field resistivity at 300 K (8.32 Ω cm) is similar to Mn_2MnReO_6 (6.80 Ω cm at 300 K).[17] Mn_2CoReO_6 shows semiconductor-like behaviour and the temperature-dependence of resistivity could be fitted by a variable-range hopping model ($T_0^{1/2}$ = 157.04 $K^{1/2}$ $\rho_0 = 6.208 \times 10^{-4}$ Ω cm, see ESI†) for $T > 60$ K (below which Mn_2CoReO_6 becomes too resistive). The temperature-dependent

resistivity measured under a magnetic field of 7 T results were practically identical to those measured at 0 T, confirming a lack of magnetoresistance.

Low temperature NPD data were used to investigate the magnetic ordering further. On cooling below ~100 K, additional magnetic Bragg reflections, consistent with magnetic ordering vector k = (1/2 1/2 0), were observed and increased in intensity on cooling. ISODISTORT[30] was used to explore possible magnetic structures and while irreps mD1 + mD2 only allowed magnetic moments on the A-sites, mD1 − mD2 gave antiferromagnetic models with moments on Mn_A as well as Co_B and Re_B sites. The 'mode inclusion' method[31,32] was used to consider possible symmetry adapted magnetic modes (by this method, the improvement in fit between observed and calculated diffraction patterns is compared for possible magnetic models). This analysis indicated ordered moments on all three sites. At temperatures down to ~50 K, the best fit was obtained with Co_B and $Re_{B'}$ moments along [010] (with constraints to give equal moments for all crystallographically equivalent sites). The Co_B and $Re_{B'}$ moments were strongly correlated in refinements (as noted for the B site ions in Mn_2MnReO_6[16]) and so the $Re_{B'}$ moment was constrained to be collinear and a third of the magnitude of the Co_B moment. The absolute orientation of the Mn_A site moments is hard to determine from powder diffraction data due to peak overlap and the slight monoclinic distortion. Good fits were obtained with Mn_A moments close to the [101], although other models of the same symmetry cannot be ruled out. This model, with collinear Mn_A moments nearly perpendicular to the B/B′-site moments, suggests two magnetic sublattices only weakly coupled and is consistent with the $M(H)$ measurements that suggest a non-null anisotropy of the antiferromagnetic structure. This magnetic model was used in subsequent sequential refinements using data collected on warming (see ESI†). This magnetic structure can also be described using the smaller triclinic cell of $P_s\bar{1}$ symmetry with basis (−1 1 −1)(−1 1 0)(0 2 0) relative to the nuclear unit cell. Final refinement details and bond lengths at 60 K are given in Tables ESI10.1–10.3 (ESI†), and refinement profiles and illustration of the 60 K magnetic structure are shown in Fig. 3.

While most magnetic reflections increase smoothly on cooling (see ESI†), some very weak reflections (at the gamma point, and indexed by the nuclear unit cell) are only observed at lower temperatures (*e.g.* 110 reflection observed below 40 K). We note that this is close in temperature to the FM-like feature suggested by magnetic susceptibility measurements and may indicate a second magnetic transition on cooling, although the feature in susceptibility measurements may also be attributed to the trace of ferrimagnetic impurity or by domain effects. The additional magnetic reflections observed for $T < 40$ K require some extra component described by a gamma point irrep of the parent structure, and all such possible magnetic modes on either the A or B/B′-sites were considered. It is likely that this component arises from the Co_B site, because the ordered moment on this site shows an anomaly around 40 K (Fig. ESI11.2, ESI†), but none of our models gave significant improvement in fit. A single peak is observed in heat capacity data at 94 K, which suggests a single magnetic phase transition in the bulk material. However, we note a slight change in the slope of heat capacity and a change in the lattice parameters, particularly the monoclinic β angle, at ~40 K are observed (Fig. ESI9.1, ESI†). This may indicate a change in magnetic behaviour correlated with a slight structural change *e.g.* magnetic phase segregation, perhaps resulting from the cation Mn–Co antisite disorder. Further analysis to understand this low temperature magnetism is needed.

The 60 K magnetic structure described above is similar to that reported for Mn_2MnReO_6[16] in that spins on both the A and B sites are close to perpendicular. This implies that, despite description by the same irreducible representation, the coupling between the A and B/B′ sublattices in Mn_2CoReO_6 is weak. This might explain the difference in transport properties between

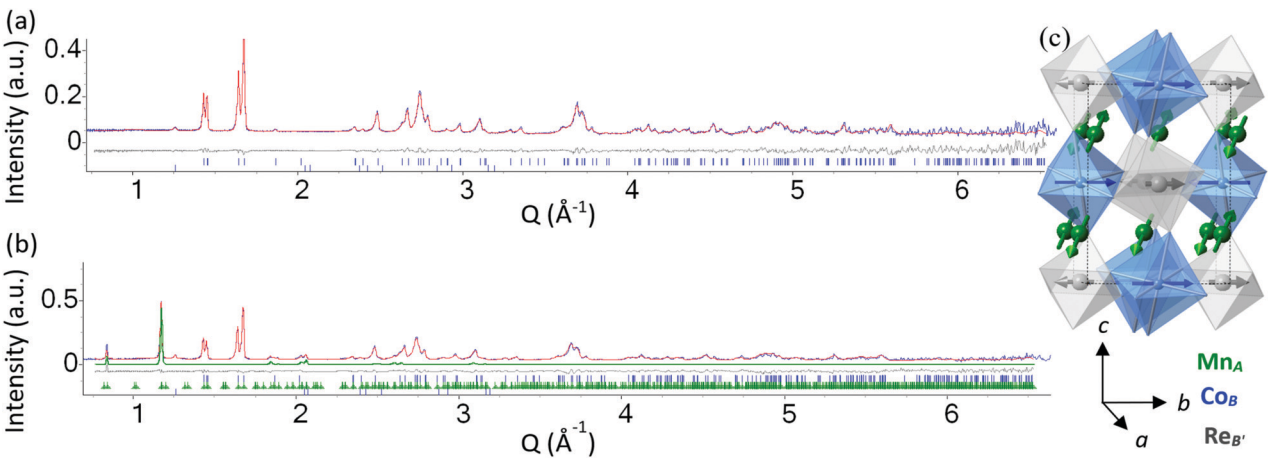

Fig. 3 Refinement profiles for Mn_2CoReO_6 using (a) 200 K NPD data (upper and lower blue ticks show peak positions for the main phase Mn_2CoReO_6 and for $Mn_{3-x}Co_xO_4$ (fitted with Pawley phase), respectively) and (b) 60 K NPD data showing 58° bank data (upper, middle and lower ticks show peak positions for nuclear and magnetic phases and $Mn_{3-x}Co_xO_4$ Pawley phase, respectively). Observed, calculated and difference profiles are shown in blue, red and grey, respectively and in (b), magnetic scattering is highlighted in green. (c) 60 K magnetic structure with Mn_A, Co_B and $Re_{B'}$ moments in green, blue and grey, respectively (oxygens omitted for clarity).

semiconducting Mn_2CoReO_6 (with no magnetoresistance) and the half-metallic Mn_2FeReO_6.[18] From the evolution of the Mn_A and Co_B site moments and magnetic peak intensities (see ESI†), these two sublattices may order at slightly different temperatures, with the Co_B site ordering a few Kelvin above the Mn_A sublattice (analogous to the magnetic ordering reported for Mn_2MnReO_6[16]), but NPD data collected at smaller temperature intervals would be necessary to confirm this. The low moment observed for the Co^{2+} site from NPD is surprising and may indicate deficiencies of our model; the low temperature magnetic behaviour is not yet understood and the change in magnetic behaviour suggested by magnetic susceptibility measurements below ~40 K may arise from the B-site ions and further investigations are needed.

In conclusion, we have studied the nuclear and magnetic structures of Mn_2CoReO_6. Transport measurements suggest that Mn_2CoReO_6 is an Efros–Shklovskii variable-range-hopping semiconductor with negligible magnetoresistance. Magnetization versus temperature measurements over fields from 0.5 T–7 T indicate that the transition at 94 K is very robustly antiferromagnetic. According to NPD, all the magnetic cations order with a k = (1/2 1/2 0) propagation vector below ~100 K. The Mn A-site cations order with moment close to the [101] direction, whereas the B/B′ cations order along the [010] direction. The different moment directions indicate a weak inter-sublattice coupling. NPD data suggests a possible second magnetic transition at ~40 K, with propagation vector k = 0, likely due to a spin reorientation involving the B/B′ ions, but further investigation is required to fully understand this transition. Future investigations, such as first principles calculations and further neutron experiments, will help to understand the electronic and magnetic structures.

This work was supported by the NSF-DMR-1507252 grant. Work at Brookhaven National Laboratory was supported by the DOE BES (DE-SC0012704) on the NSLS-II Beamlines 7BM and 6BM. We would like to thank Ms J. Hanley at LDEO in Columbia Univ. for making the high-pressure assemblies. EEM and VAC are grateful to the Leverhulme Trust (RPG-2017-362) for funding. The authors acknowledge the Science and Technology Facility Council (UK) for the provision of neutron beam time at the ISIS facility on the WISH instrument (DOI: 10.5286/ISIS.E.101137712). M. X. Wu was supported by the National Natural Science Fund of China (NSFC-11804404).

Conflicts of interest

The authors declare that there are no conflicts of interest.

Notes and references

1 H. N. Khan, D. A. Hounshell and E. R. H. Fuchs, *Nat. Electron.*, 2018, **1**, 14–21.
2 T. N. Theis and H.-S. P. Wong, *Comput. Sci. Eng.*, 2017, **19**, 41–50.
3 K. I. Kobayashi, T. Kimura, H. Sawada, K. Terakura and Y. Tokura, *Nature*, 1998, **395**, 677.
4 W. H. Baur, W. Joswig, G. Pieper and D. Kassner, *J. Solid State Chem.*, 1992, **99**, 207–211.
5 M. Retuerto, F. Jiménez-Villacorta, M. J. Martínez-Lope, Y. Huttel, E. Roman, M. T. Fernández-Díaz and J. A. Alonso, *Phys. Chem. Chem. Phys.*, 2010, **12**, 13616–13625.
6 A. K. Paul, M. Jansen, B. Yan, C. Felser, M. Reehuis and P. M. Abdala, *Inorg. Chem.*, 2013, **52**, 6713–6719.
7 J. S. Park, B. J. Han, C. S. Kim and B. W. Lee, *J. Magn. Magn. Mater.*, 2001, **226–230**, 741–742.
8 K. I. Kobayashi, T. Kimura, Y. Tomioka, H. Sawada, K. Terakura and Y. Tokura, *Phys. Rev. B: Condens. Matter Mater. Phys.*, 1999, **59**, 11159–11162.
9 D. D. Sarma, P. Mahadevan, T. Saha-Dasgupta, S. Ray and A. Kumar, *Phys. Rev. Lett.*, 2000, **85**, 2549–2552.
10 S. E. Lofland, T. Scabarozi, Y. Moritomo and S. Xu, *J. Magn. Magn. Mater.*, 2003, **260**, 181–183.
11 S. Vasala and M. Karppinen, *Prog. Solid State Chem.*, 2015, **43**, 1–36.
12 M. W. Lufaso and P. M. Woodward, *Acta Crystallogr., Sect. B: Struct. Sci.*, 2001, **57**, 725–738.
13 A. A. Belik and W. Yi, *J. Phys.: Condens. Matter*, 2014, **26**, 163201.
14 M. Retuerto, S. Skiadopoulou, F. Borodavka, C. Kadlec, F. Kadlec, J. Prokleška, Z. Deng, J. A. Alonso, M. T. Fernandez-Diaz, F. O. Saouma, J. I. Jang, D. Legut, S. Kamba and M. Greenblatt, *Phys. Rev. B*, 2018, **97**, 144418.
15 A. Hossain, P. Bandyopadhyay and S. Roy, *J. Alloys Compd.*, 2018, **740**, 414–427.
16 A. M. Arevalo-Lopez and J. P. Attfield, *Chem. Commun.*, 2016, **52**, 5558.
17 M.-R. Li, J. P. Hodges, M. Retuerto, Z. Deng, P. W. Stephens, M. C. Croft, X. Deng, G. Kotliar, J. Sanchez-Benitez, D. Walker and M. Greenblatt, *Chem. Mater.*, 2016, **28**, 3148–3158.
18 M. R. Li, M. Retuerto, Z. Deng, P. W. Stephens, M. Croft, Q. Huang, H. Wu, X. Deng, G. Kotliar, J. Sánchez-Benítez, J. Hadermann, D. Walker and M. Greenblatt, *Angew. Chem., Int. Ed.*, 2015, **54**, 12069–12073.
19 A. M. Arévalo-López, G. M. McNally and J. P. Attfield, *Angew. Chem., Int. Ed.*, 2015, **54**, 12074–12077.
20 M.-R. Li, P. W. Stephens, M. Croft, Z. Deng, W. Li, C. Jin, M. Retuerto, J. P. Hodges, C. E. Frank, M. Wu, D. Walker and M. Greenblatt, *Chem. Mater.*, 2018, **30**, 4508–4514.
21 M. Retuerto, M.-R. Li, P. W. Stephens, J. Sánchez-Benítez, X. Deng, G. Kotliar, M. C. Croft, A. Ignatov, D. Walker and M. Greenblatt, *Chem. Mater.*, 2015, **27**, 4450–4458.
22 M. Retuerto, M. J. Martínez-Lope, M. García-Hernández, M. T. Fernández-Díaz and J. A. Alonso, *Eur. J. Inorg. Chem.*, 2008, 588–595.
23 A. Nag, J. Manjanna, R. M. Tiwari and J. Gopalakrishnan, *Chem. Mater.*, 2008, **20**, 4420–4424.
24 H. L. Cuthbert, J. E. Greedan and L. Cranswick, *J. Solid State Chem.*, 2006, **179**, 1938–1947.
25 Z. Zhang, C. J. Howard, B. J. Kennedy, K. S. Knight and Q. Zhou, *J. Solid State Chem.*, 2007, **180**, 1846–1851.
26 H. Kato, T. Okuda, Y. Okimoto, Y. Tomioka, K. Oikawa, T. Kamiyama and Y. Tokura, *Phys. Rev. B: Condens. Matter Mater. Phys.*, 2004, **69**, 184412.
27 G. Popov, V. Lobanov, E. V. Tsiper, M. Greenblatt, E. N. Caspi, A. Borissov, V. Kiryukhin and J. W. Lynn, *J. Phys.: Condens. Matter*, 2004, **16**, 135.
28 V. F. Sears, *Neutron news*, 1990, **3**, 29–37.
29 R. D. Shannon, *Acta Crystallogr., Sect. A: Cryst. Phys., Diffr., Theor. Gen. Crystallogr.*, 1976, **32**, 751.
30 B. J. Campbell, H. T. Stokes, D. E. Tanner and D. M. Hatch, *J. Appl. Crystallogr.*, 2006, **39**, 607–614.
31 A. J. Tuxworth, E. E. McCabe, D. G. Free, S. J. Clark and J. S. O. Evans, *Inorg. Chem.*, 2013, **52**, 2078–2085.
32 E. E. McCabe, C. Stock, E. E. Rodrigues, A. S. Wills, J. W. Taylor and J. S. O. Evans, *Phys. Rev. B: Condens. Matter Mater. Phys.*, 2014, **89**, 100402(R).

